# Internal barrier layer capacitor, nearest neighbor hopping, and variable range hopping conduction in Ba1–x Sr x TiO3–$\delta$ nanoceramics

Soumitra Sulekar, Ji Hyun Kim, Hyuksu Han, Pascal Dufour, Christophe Tenailleau, Juan Claudio Nino, Eloisa Cordoncillo, Hector Beltran-Mir, Sébastien Dupuis, Sophie Guillemet

# Internal barrier layer capacitor, nearest neighbor hopping, and variable range hopping conduction in $Ba_{1-x}Sr_xTiO_{3-\delta}$ nanoceramics

Soumitra Sulekar[1], Ji Hyun Kim[1], Hyuksu Han[2,4], Pascal Dufour[2], Christophe Tenailleau[2], Juan Claudio Nino[1], Eloisa Cordoncillo[3], Hector Beltran-Mir[3], Sébastien Dupuis[2], and Sophie Guillemet-Fritsch[2,*]

[1] *Department of Materials Science and Engineering, University of Florida, Gainesville, FL 32611, USA*
[2] *CIRIMAT, Université de Toulouse, UMR CNRS-UPS-INP 5085, 118 route de Narbonne, 31062 Toulouse Cedex 9, France*
[3] *Departamento de Química Inorgànica i Orgànica, Universitat Jaume I, 12071 Castellon, Spain*
[4] *Korea Institute of Industrial Technology (KITECH), 137-41 Gwahakdanji-ro, Gangneung-si, Gangwon-Do 25440, Republic of Korea*

## ABSTRACT

The dielectric properties of the solid solution $Ba_{1-x}Sr_xTiO_{3-\delta}$ ($0 \leq x \leq 1$) have been investigated. The nanopowders were prepared via a coprecipitation reaction followed by a calcination treatment. Spark plasma sintering allowed to obtain dense nanocrystalline ceramics. Broadband impedance spectroscopy revealed colossal permittivity ($\varepsilon' = 10^5$) associated with low losses ($\tan \delta = 0.03$) in the most favorable case. The bulk conductivity data was analyzed using Jonscher's universal dielectric response model. In the Ba-rich compound, conduction process followed variable range hopping conduction model while the Sr-rich BST compound showed the nearest neighbor hopping conduction mechanism associated with displacements of space charges. These two different conduction mechanisms might be able to explain superior temperature–frequency-independent dielectric properties in Sr-rich BST compound compared to Ba-rich BST compound.

## Introduction

Colossal permittivity compounds have been intensively studied during the last decade because of their high technological potential, especially as dielectrics for capacitor applications. These materials, usually metal oxides, can be fabricated as bulk materials and/or thin films. Literature shows that different techniques have been used to achieve high dielectric response in such materials [1–6]. One commonly used method is the construction of superlattices as has been shown by O'Neill et al. [1] for $Ba_{0.8}Sr_{0.2}TiO_3$ and $Ba_{0.2}Sr_{0.8}TiO_3$ and by Zubko et al. for $PbTiO_3$/$SrTiO_3$ thin film structures [2]. Multilayers and graded structures have also been used to elicit high permittivity [3, 4]. Cole et al. have shown that low

Address correspondence to E-mail: guillem@chimie.ups-tlse.fr

DOI 10.1007/s10853-016-0019-0

losses and low leakage current can be obtained using a buffer layer of strontium titanate on top of barium strontium titanate films [5]. Similarly, Tagantsev et al. have evidenced via modeling for bulk materials that a layered composite of ferroelectrics and dielectrics can give low loss values which are relatively independent of the permittivity [6]. An ideal colossal permittivity material should exhibit wide windows with temperature- and frequency-independent response. Among bulk materials, different oxides such as $CaCu_3Ti_4O_{12}$ (CCTO) [8–12], Li–Ti co-doped NiO [13], ferrites [14] [15], or reduced perovskites [16, 17], show a remarkably high dielectric permittivity which is temperature and frequency independent in a broad range. Such high permittivity is attributed to a number of intrinsic and extrinsic interfacial mechanisms. For example, Lunkenheimer et al. [12, 18] have shown that polarization effects at the electrode and material contact contribute to the apparent high dielectric constant values in CCTO. The intrinsic contribution on the other hand is attributed to hopping polarization, depletion layers [19], and insulating domain and grain boundaries with respect to semiconducting grains and domains [20]. Moreover, in the case of barium titanate (BT), the electrode effect has been separated out to be about 15 % by Han et al. [21]. Noble metals like Au and Ag form Schottky contacts with BT, whereas Al electrodes form ohmic contacts. The electrode effect on colossal permittivity can thus be estimated by subtracting the permittivity obtained for Al electrode from that measured with Au. Overall, it was shown that for barium titanate, depending on processing conditions, the relative contributions to colossal permittivity are 65 % hopping polarization, ∼20 % interfacial polarization, and ∼15 % electrode effects [21].

It is important to note that a hopping polarization process induces a Maxwell–Wagner polarization between semiconducting grains and insulating grain boundaries, due to a high number of charge carriers. This heterogeneous spatial charge distribution mainly contributes to the significant increase of permittivity in materials at low frequencies. This behavior, which is well described by the internal barrier layer capacitor model (IBLC), can be represented by Koop's equivalent circuit [22] with the two contributions of grains and grain boundaries in series.

To further expand on recent demonstrations of induced colossal effective permittivity in $BaTiO_3$-based ceramics, the present work focuses on the dielectric properties of $Ba_{1-x}Sr_xTiO_{3-\delta}$ (BST $0 \leq x \leq 1$) bulk ceramics for enhanced capacitive applications. In a previous paper, we have investigated the colossal effective permittivity and low losses in BST nanoceramics [23]. Polaron hopping mediated by $Ti^{+3}$ ions and oxygen vacancies is the main contributing mechanism to colossal permittivity in barium-rich BST. In this work, to clarify the conduction mechanisms in dense bulk BST, we briefly present the structural and microstructural characteristics of $Ba_{1-x}Sr_xTiO_{3-\delta}$ (BST $0 \leq x \leq 1$) and then focus on relationships between colossal permittivity and bulk conduction processes in the systems. Using impedance spectroscopic analysis, impedance complex plane plots allow to point out the inhomogeneous distribution of space charges between grains and grain boundaries. In addition, based on the impedance data analysis using appropriate Koop's equivalent circuit model [22], we show that the grain boundaries are insulating while the grains still remain conductive after sintering process combined with annealing post-sintering treatment. Two different conduction mechanisms namely, variable range hopping (VRH) and nearest neighbor hopping (NNH) are investigated to explain the temperature and frequency independence of the materials under consideration.

## Materials and method

### Powder Synthesis and Spark Plasma Sintering

The coprecipitation method was used to prepare the BST nanopowders, as detailed previously [24]. $BaCl_2{\cdot}2H_2O$ (Prolabo), $SrCl_2{\cdot}6H_2O$ (Aldrich), and lab-made $TiOCl_2$ were weighed in appropriate proportions, dissolved in water, and added to an ethanolic oxalic acid solution. After a 5-h aging, the solution was centrifuged and dried for 12 h at 80 °C. The powders were then grinded and sieved before calcination at 850 °C for 4 h. Spark plasma sintering (SPS) was carried out using a Dr. Sinter 2080 device from Sumitomo Coal Mining (Fuji Electronic Industrial, Saitama, Japan) in order to densify the BST nanopowders. The optimized sintering procedure has been reported in a previous work [25]. The oxide powder (0.5 g) was loaded in the graphite die (8 mm

diameter) and the powders were sintered at 1150 °C in vacuum (residual cell pressure <10 Pa). The powders were heated at a rate of 25 °C/min, and a 3-min dwell time was applied at 1150 °C before the electric current was switched off and the pressure was released. A thin carbon layer, due to graphite contamination from the graphite sheets, was observed on the as-sintered pellets surfaces [26] and was removed by polishing the surface. Finally, SPS ceramics were annealed 15 min at 850 °C in oxidizing atmosphere and quenched in air.

## Material Characterization

Inductively coupled plasma-atomic emission spectroscopy (ICP-AES) was used to determine the chemical composition of the different oxide powders with a JY 2000 device (Horiba Jobin–Yvon, Kyoto, Japan). The morphology of the powders was observed with a field emission gun scanning electron microscope (FEG-SEM, JSM 6700F, JEOL, Tokyo, Japan) and the particle size determined by Image J [27]. Therefore, we used the linear intercept method standard (ASTM E112) to measure the grain size of the ceramics. The crystalline structure and phase purity were investigated at room temperature by X-ray diffraction analysis using a D4 Endeavor X-ray diffractometer ($CuK_{\alpha 1} = 0.154056$ nm and $CuK_{\alpha 2} = 0.154044$ nm; Bruker AXS, Karlsruhe, Germany) from 20° to 80° (2-theta). Archimedes method was used to determine the density of the ceramics (ARJ 220-4 M balance, KERN, Murnau-Westried, Germany). Thin gold electrodes (thickness ~30 nm) were sputtered (108 Auto, Cressington Scientific Instruments, Watford, U.K.) on the pellets surface. Impedance measurements were recorded over the frequency range 10 Hz to 13 MHz and the temperature range 120–473 K using an Alpha-N Novocontrol impedance analyzer, with an *ac* voltage of 0.1 V. Impedance data were corrected for overall pellet geometry and for the blank cell capacitance (jig correction). For low-temperature impedance data measurements, the electroded samples were placed in a closed cycle cryogenic workstation (CTI 22, Cryo Industries of America, Manchester, NH) and measurements were performed as a function of frequency (40 Hz–100 kHz) from 300 to 40 K (20 K step size) using an Agilent 4284A LCR meter under an applied *ac* voltage of 1 V.

# Results and discussion

## Structural and microstructural characterization

Figure 1 shows the FEG-SEM micrographs of starting powders and dense ceramics of $Ba_{0.8}Sr_{0.2}TiO_{3-\delta}$ and $Ba_{0.2}Sr_{0.8}TiO_{3-\delta}$ compounds. Powders are homogeneous in shape and size as described in a previous paper [23]. Nanometer size of grains is preserved after SPS process and densities higher than 98 % of the theoretical densities are obtained.

The thickness of the grain boundary, i.e., 1 nm, was evaluated from HR-TEM images of a $BaTiO_{3-\delta}$ dense ceramic (Fig. 2).

X-ray diffraction patterns of BST nanoceramics ($0 \leq x \leq 1$) are presented in Fig. 3. Each composition crystallizes in the perovskite structure without any additional phase for both powders and pellets. The shift of Bragg's peaks as composition changes is a result of an effective substitution between Ba and Sr, leading to a decrease of the lattice parameters from 4 Å for $BaTiO_{3-\delta}$ to 3.9 Å for $SrTiO_{3-\delta}$.

## Impedance measurements

In order to characterize the electrical properties of the samples, and therefore, to analyze the behavior of the different regions of the samples, i.e., grains and grain boundaries, impedance measurements were carried out as a function of frequency over the temperature range from 120 to 473 K.

Analysis of the impedance complex plane, Z*, plots, Fig. 4a and b, for a high Ba-content sample and a high Sr-content sample at 170 K, showed an asymmetric arc of resistance $R_1$ at high frequencies ($2 \times 10^5$) with a distortion from ideal semi-circular shape for both compositions.

Assignment of the main impedance arc to grain regions is supported by the representation of the same impedance data as Z″/M″ spectroscopic plots, Fig. 4c and d. The peak in the M″ plot corresponds to the region of the sample with the smallest capacitance ($2.8 \times 10^{-10}$ F cm$^{-1}$ for $Ba_{0.8}Sr_{0.2}TiO_{3-\delta}$ and $2 \times 10^{-10}$ F cm$^{-1}$ for $Ba_{0.2}Sr_{0.8}TiO_{3-\delta}$), and therefore, to the grains. Thus, $R_1$ corresponds to the sample bulk resistance and is in the order of 3500 Ω cm for $Ba_{0.8}Sr_{0.2}TiO_{3-\delta}$ and 7500 Ω cm for $Ba_{0.2}Sr_{0.8}TiO_{3-\delta}$ at 170 K.

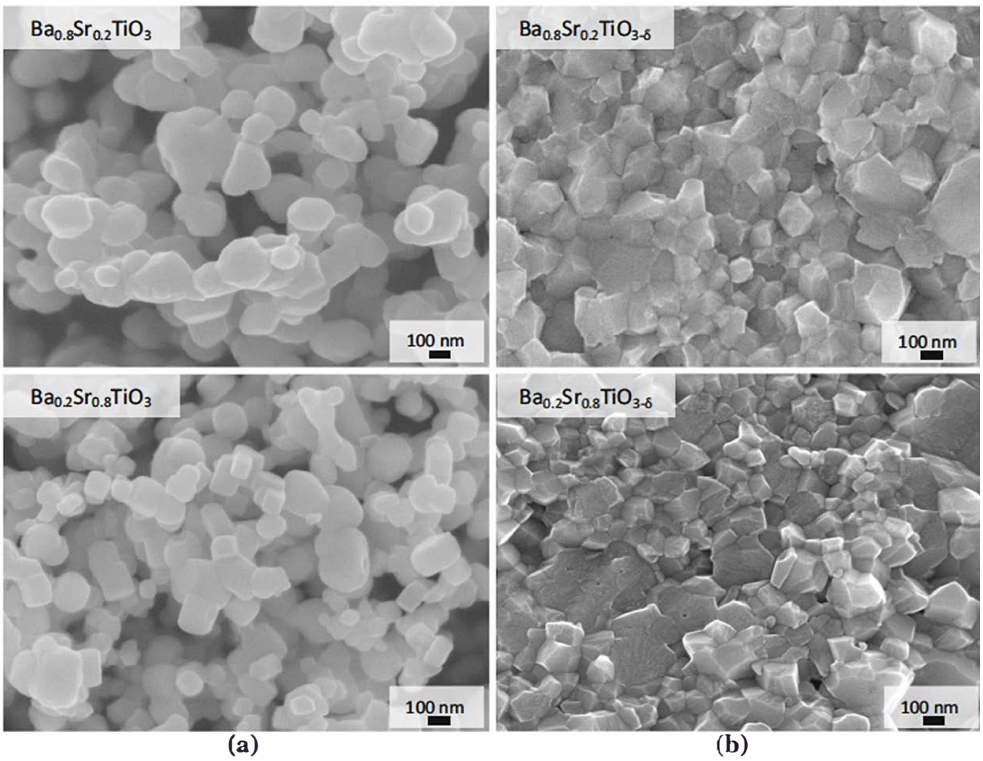


**Figure 1** MEB FEG micrographs of $Ba_{0.8}Sr_{0.2}TiO_3$ and $Ba_{0.2}Sr_{0.8}TiO_3$ powders (a) and fractured ceramics (b).

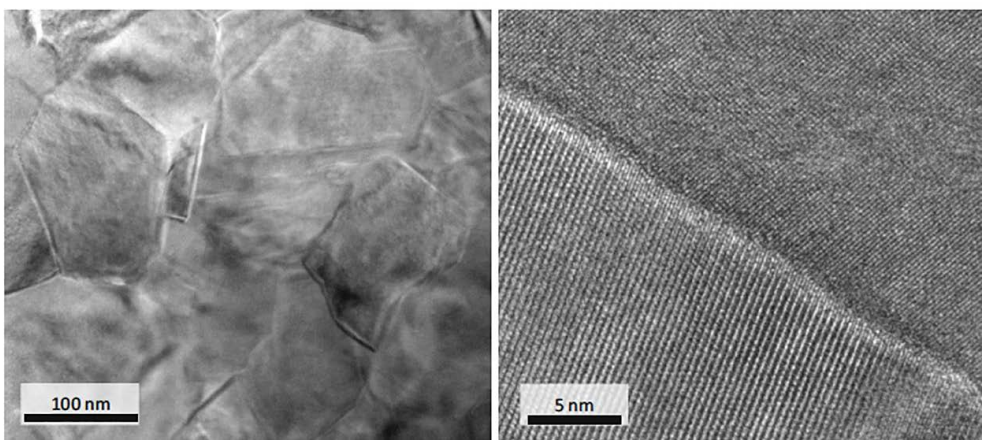


**Figure 2** HREM TEM micrographs of $BaTiO_{3-\delta}$ nanoceramic.

The same data represented as spectroscopic plots of capacitance, C′, Fig. 4e and f, demonstrate an almost frequency-independent, but temperature-dependent plateau at high frequencies for both samples which is attributed to the sample bulk, $C_1$. The values of capacitance are roughly around $2.8 \times 10^{-10}$ F cm$^{-1}$ and $2 \times 10^{-10}$ F cm$^{-1}$ at 170 K for $Ba_{0.8}Sr_{0.2}TiO_{3-\delta}$ and $Ba_{0.2}Sr_{0.8}TiO_{3-\delta}$, respectively. A second plateau is observed at lower frequency with capacitance $1 \times 10^{-8}$ F cm$^{-1}$ and $6.5 \times 10^{-9}$ F cm$^{-1}$ at 170 K for $Ba_{0.8}Sr_{0.2}TiO_{3-\delta}$ and $Ba_{0.2}Sr_{0.8}TiO_{3-\delta}$, respectively, which might be attributed to a conventional (but high permittivity) grain boundary, $C_2$. Therefore, for both samples, the impedance data may be represented ideally by an equivalent circuit containing two parallel RC elements in series.

## Internal barrier layer capacitor (IBLC) model

The IBLC model can be described by Koop's equivalent circuit consisting of capacitive, conductive, and a constant phase elements in parallel and/or in

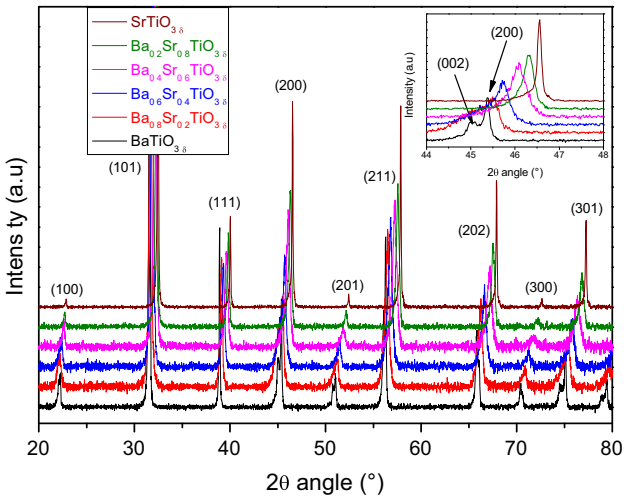


**Figure 3** XRD patterns of $Ba_{1-x}Sr_xTiO_{3-\delta}$ ($0 \le x \le 1$) ceram ics; *inset*: 44 48° 2θ angle enlargement.

series. For colossal permittivity materials, electrical heterogeneities between grains and grain boundaries drive the properties [10]. According to the Koop's equivalent circuit, the grain and grain boundary responses are built in series and each part is composed of a ($C_{g/gb}$, $\sigma_{g/gb,dc}$) parallel circuit, described by the following equation [28]:

$$\varepsilon^* = \frac{\left[C_g(i\omega)^{1\ P_g} + \sigma_{g,dc} + i\omega\varepsilon_\infty\varepsilon_0\right]\left[C_{gb}(i\omega)^{1\ P_{gb}} + \sigma_{gb,dc} + i\omega\varepsilon_\infty\varepsilon_0\right](1+\eta)}{i\varepsilon_0\omega\left\{C_{gb}(i\omega)^{1\ P_g}b + \sigma_{gb,dc} + \eta\left[C_g(i\omega)^{1\ P_g} + \sigma_{g,dc}\right]\right\} \quad \omega^2\varepsilon_\infty\varepsilon_0^2(1+\eta)}, \tag{1}$$

where $\sigma_{g,dc}$ is the dc conductivity of grain and $\sigma_{gb,dc}$ is the dc conductivity of grain boundary in the frequency-independent part of Jonscher's model. $\varepsilon_{0/\infty}$, i, ω, and η are, respectively, the permittivity of vacuum/sample at infinite frequency, the imaginary unit, the angular frequency, and the ratio of grain boundary thickness on average grain size. In addition, Eq. 1 points out a $P_{g/gb}$ contribution representing the conductive and capacitive trends of grains and grain boundaries. A value of $P$ close to 1 indicates a conductive behavior while a value close to 0 implies a capacitive response. Finally, $C_{g/gb}$ is a function of $P_{g/gb}$, as given by the Eq. 2:

$$C_{g/gb} = \sigma_{g/gb,0}/\left[0.5\pi\cos\left(1 - P_{g/gb}\right)\right], \tag{2}$$

where $\sigma_{g/gb,0}$ is the static conductivity of grains/grain boundaries.

Experimental data for $Ba_{1-x}Sr_xTiO_{3-\delta}$ nanoceramics ($0 \le x \le 1$) are plotted in Fig. 5 and the fitted curves using Eq. 1 are presented. The different fitting parameters ($P_{g/gb}$, $\sigma_{g/gb}$, $C_{g/gb}$, η, and $\varepsilon_\infty$) are shown in Table 1. For all the compositions, they are in good agreement with the experimental data ($R^2 > 0.997$, except for $SrTiO_3$ $R^2 = 0.950$). As discussed in our previous paper [23], the electrical properties of $SrTiO_3$ are not driven by the thermally activated hopping polaron model, and thus, we will exclude this particular composition in the following discussion.

The values of $P_g$ of all the compounds are close to 1 and those of $P_{gb}$ are close to 0, indicating a conductive response of the grains and a capacitive response of grain boundaries. Moreover, $\sigma_{g,dc}$ are at least two orders of magnitude higher than $\sigma_{gb,dc}$, which is in accordance with the IBLC model. In addition, the values of $C_g/C_{gb}$ support the fact that grains are conductive (or semiconductive) while grain boundaries are insulating.

Finally, a simple comparison between the six compositions could give us some general trends about Ba–Sr substitution on electrical properties. In fact, we observe a quasi-constant value of $P_g$ ($\approx$0.92) until $x = 0.4$, then $P_g$ substantially decreases as $x$ increases above 0.4. This means that the grain conductivity behavior is similar for the 3 highest Ba-content nanoceramics, while this conductive behavior drastically decreases for the three other samples (i.e., Sr-rich BST compound). However, $P_{gb}$ is almost constant for all the compositions, showing a similar trend of grain boundaries to be capacitive. $\sigma_{gb,dc}$ shows a slow decrease as Sr content increases from 0 to 0.4, then drastically decreases for higher Sr concentration. The values of $C_g$ and $C_{gb}$ related with $P_g$ and $P_{gb}$ decrease when $x$ increases. η is constant ($\approx 1 \times 10^{-2}$), indicating a grain boundary thickness 100 times smaller than the grain size, which is consistent with the results determined from HREM-TEM observations (Fig. 2): The grain size of the $BaTiO_{3-\delta}$ nanoceramic lies between 100 and 250 nm, and the grain boundaries thickness was estimated to be 1 nm. Lastly, $\varepsilon_\infty$, corresponding to the permittivity at infinite frequency remains quasi-constant for all the compositions tested.

## Universal dielectric response (UDR) model

In order to further investigate the conduction mechanisms in colossal permittivity materials such as the reduced BST nanoceramics, it is necessary to link

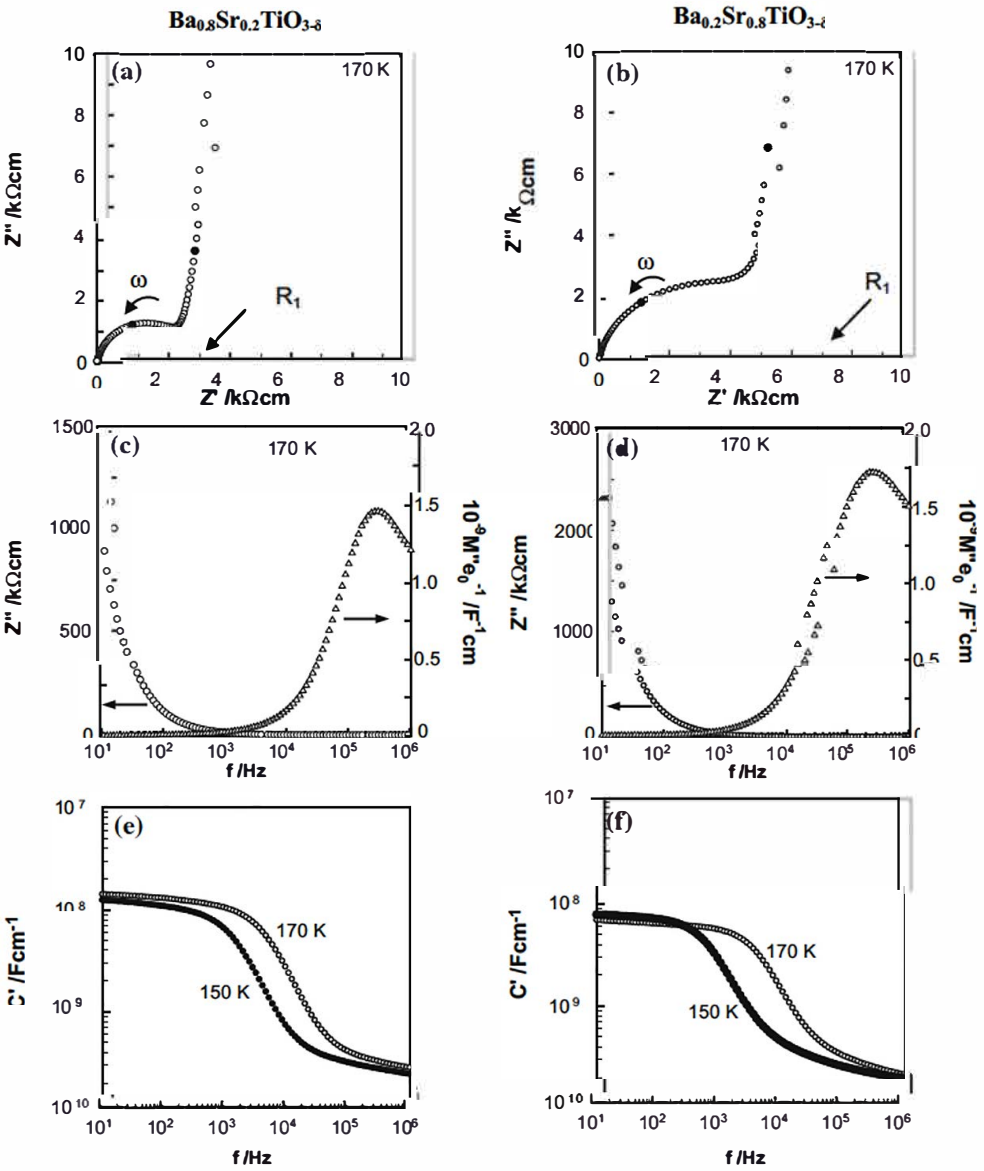


**Figure 4** Impedance complex plane plots and Z''/M'' spectroscopic plots at 170 K, and capacitance data at 150 and 170 K for $Ba_{0.8}Sr_{0.2}TiO_{3-\delta}$ (a, c and e) and $Ba_{0.2}Sr_{0.8}TiO_{3-\delta}$ (b, d and f) nanoceramics. The solid data points in (a) and (b) refer to frequencies of 200 and 4.5 kHz.

dielectric properties to the bulk conductivity ($\sigma'$), as shown in Eq. 3:

$$\sigma'(\omega) = \omega_0 \varepsilon_0 \varepsilon_r''(\omega). \quad (3)$$

The universal dielectric response (UDR) model developed by Jonscher [29] [30], established the relation between the bulk conductivity and the grains conductivity in the high frequency-independent area. In this way, by plotting the bulk conductivity as a function of frequency, it is possible to determine the dc conductivity ($\sigma_{dc}$) of the grains.

$$\sigma' = \sigma_{dc} + \sigma_0 f^s, \quad (4)$$

where $\sigma_0$ is a prefactor, f is the experimental frequency, and $s$ is a temperature-dependent constant. It is worth noting that the value of $s$ is between 0 and 1, and a value close to 1 indicates a localized polarization mechanism, while a value closer to 0 indicates charge carriers are free to move through the entire bulk. In order to better understand the electrical properties of the BST system, we will focus on two compositions: Ba-rich BST compound $Ba_{0.8}Sr_{0.2}TiO_{3-\delta}$ and Sr-rich BST compound $Ba_{0.2}Sr_{0.8}TiO_{3-\delta}$, since these two compounds show the most distinct dielectric behavior from each other.

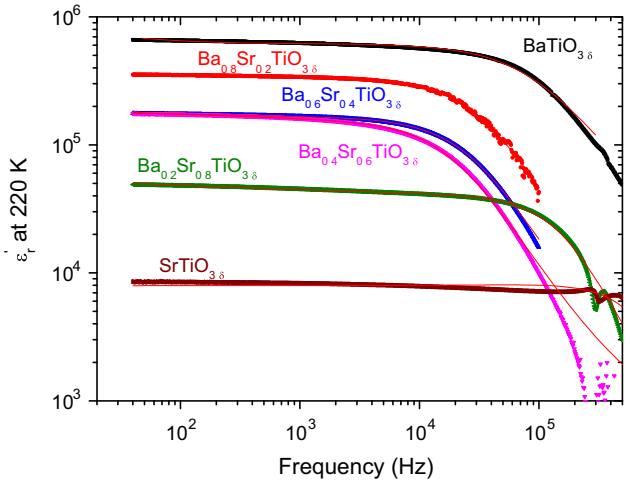


**Figure 5** BST permittivity data fitted with IBLC model.

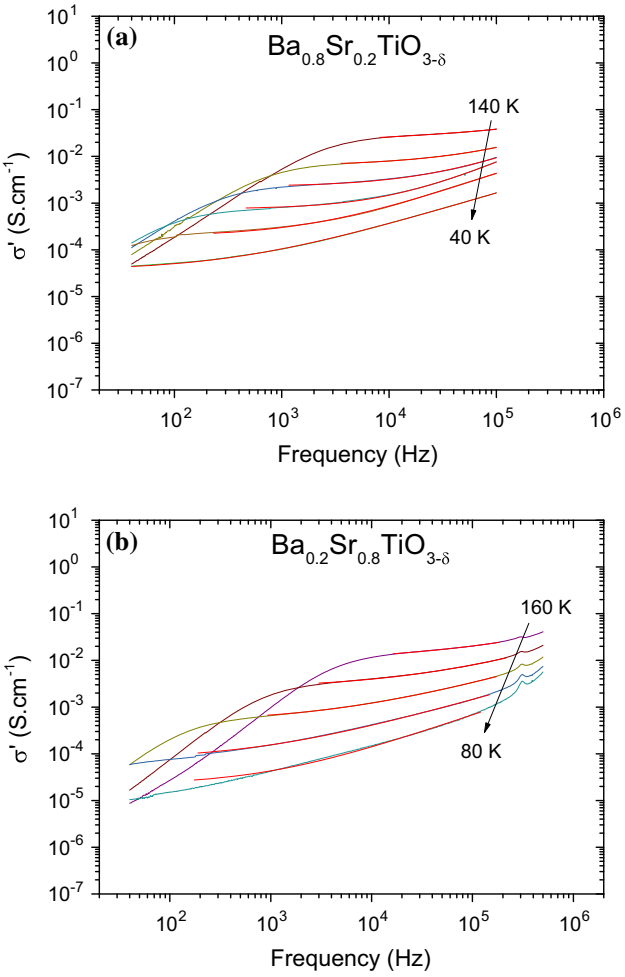


**Figure 6** Frequency dependence of the conductivity at different temperatures for **a** $Ba_{0.8}Sr_{0.2}TiO_{3-\delta}$ and **b** $Ba_{0.2}Sr_{0.8}TiO_{3-\delta}$.

σ′ versus $f$ curves are plotted for different temperatures and the corresponding fitting curves extracted from Eq. 4 are presented in Fig. 6 for these two compositions. The results for fitting parameters are also presented in Table 2. As can be seen in Table 2, $\sigma_{dc}$ and $\sigma_0$ decrease as temperature decreases regardless of the composition. However, for $Ba_{0.8}Sr_{0.2}TiO_{3-\delta}$, $s$ values increase as temperature decreases from 140 to 80 K, then further decreases at lower temperatures, while the $s$ value is quasi-constant for $Ba_{0.2}Sr_{0.8}TiO_{3-\delta}$. These contradictory dependences of $s$ values as a function of temperature for two compositions are further investigated using the two different thermally activated hopping polaron models, the NNH and the VRH model, and the results are described in the following sections.

## Effect of Sr-Ba substitution on conduction mechanisms in BST compounds

NNH conduction model considers a constant distance of hopping between nearest neighbors, as described in Eq. 5 [31], and is based on the linear variation of ln $\sigma_{dc}$ as a function of $1/T$:

$$\sigma_{dc} = \sigma_1 \exp(-E_{A1}/kT), \quad (5)$$

where $\sigma_1$ is the pre-exponential factor dependent on the concentration and size of defects, $T$ is the absolute temperature, $E_{A1}$ is the activation energy required for

**Table 1** Fitting parameters using the IBLC model

| Composition $Ba_{1-x}Sr_xTiO_{3-\delta}$ | $P_g$ | $P_{gb}$ | $\sigma_{g,dc}$ (S/cm) | $\sigma_{gb,dc}$ (S/cm) | $C_g$ | $C_{gb}$ | η ( $t_{gb}/t_g$) | $\varepsilon_\infty$ |
|---|---|---|---|---|---|---|---|---|
| $BaTiO_{3-\delta}$ | 0.92 | 0.02 | $5.1 \times 10^{-2}$ | $5.6 \times 10^{-6}$ | 1.18 | $6.2 \times 10^{-8}$ | 0.00996 | 479 |
| $Ba_{0.8}Sr_{0.2}TiO_{3-\delta}$ | 0.92 | 0.01 | $8.1 \times 10^{-4}$ | $2.5 \times 10^{-6}$ | 0.23 | $2.9 \times 10^{-8}$ | 0.00998 | 505 |
| $Ba_{0.6}Sr_{0.4}TiO_{3-\delta}$ | 0.92 | 0.02 | $2.5 \times 10^{-3}$ | $1.9 \times 10^{-6}$ | 0.09 | $1.2 \times 10^{-8}$ | 0.00996 | 512 |
| $Ba_{0.4}Sr_{0.6}TiO_{3-\delta}$ | 0.89 | 0.04 | $2.3 \times 10^{-2}$ | $2 \times 10^{-12}$ | 0.04 | $1.4 \times 10^{-8}$ | 0.00984 | 509 |
| $Ba_{0.2}Sr_{0.8}TiO_{3-\delta}$ | 0.80 | 0.01 | 0.2 | $3.8 \times 10^{-10}$ | 0.01 | $3.5 \times 10^{-9}$ | 0.01307 | 500 |
| $SrTiO_{3-\delta}$ | 0.028 | 0.0002 | $3.3 \times 10^{-7}$ | $1.5 \times 10^{-7}$ | $10^{-7}$ | $9.9 \times 10^{-8}$ | 0.02113 | 553 |

**Table 2** Fitting parameters using the UDR model

| Composition | $T$ (K) | $\sigma_{dc}$ (S cm$^{-1}$) | $\sigma_0$ | $s$ | $R^2$ | Δf (kHz) |
|---|---|---|---|---|---|---|
| $Ba_{0.8}Sr_{0.2}TiO_{3-\delta}$ | 140 | 0.01799 | 2.1E 4 | 0.39488 | 0.99618 | 10 100 |
| | 120 | 0.00636 | 1.4E 6 | 0.76218 | 0.99919 | 3 100 |
| | 100 | 0.00227 | 3.3E 7 | 0.86625 | 0.99881 | 1 100 |
| | 80 | 7.49E 4 | 9.3E 8 | 0.97315 | 0.99949 | 0.04 100 |
| | 60 | 1.92E 4 | 4.5E 7 | 0.7935 | 0.9997 | 0.02 100 |
| $Ba_{0.2}Sr_{0.8}TiO_{3-\delta}$ | 160 | 0.00959 | 3.04E 5 | 0.50982 | 0.99865 | 20 200 |
| | 140 | 0.00262 | 5.08E 6 | 0.60553 | 0.99909 | 3 200 |
| | 120 | 4.98E 4 | 2.8E 6 | 0.60234 | 0.99983 | 1 200 |
| | 100 | 7.5E 5 | 1.13E 6 | 0.61787 | 0.99949 | 0.2 200 |
| | 80 | 2.91E 6 | 1.28E 7 | 0.74267 | 0.99821 | 0.2 200 |

the hopping polaron, and $k$ is the Boltzmann constant.

The logarithm of $\sigma_{dc}$ was plotted as a function of $1/T$ for the two compositions of $Ba_{0.8}Sr_{0.2}TiO_{3-\delta}$ and $Ba_{0.2}Sr_{0.8}TiO_{3-\delta}$ (Fig. 7), and it can be clearly seen that two different behaviors exist for the compositions. In other words, for the case of the Sr-rich composition, the variation of the grain's conductivity with temperature fits well with the NNH model. The calculated activation energy, 0.110 eV, is in agreement with a hopping conduction process occurring between nearest neighbors [32, 33]. Moreover, this value is in the same range of the value of 0.165 eV, determined using Debye model. On the other hand, the Ba-rich composition does not follow NNH model and conductivity values deviate from the linear relationship with $1/T$ as temperature decreases. In this latter case, one can consider VRH model, in which the activation energy and the hopping distances of charge carriers are temperature dependent [34].

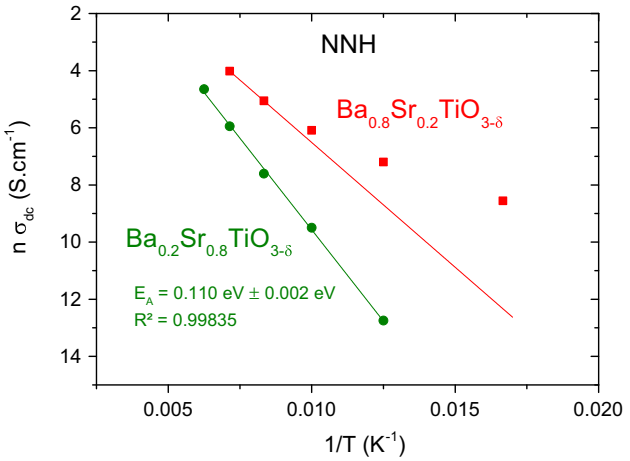


**Figure 7** NNH model applied to BST nanoceramics.

This behavior was pointed out for the first time by Mott [34] and leads to an $\exp(-T_0/T)^p$ conductivity dependence, as described in Eqs. 6 and 7.

$$\sigma_{dc} = \sigma_2 \exp[-(T_0/T)^p] \tag{6}$$

$$T_0 = \left[24/\pi\alpha^3 kN(E_F)\right], \tag{7}$$

where $\sigma_2$ is the pre-exponential constant dependent on the defect concentration and size, α is the length of the localized wave function, and $N(E_F)$ is the number of electrons per unit volume within a range of the Fermi level. Generally, the reported $p$ exponent equals 1/4 (or 1/3 in two dimensions) as observed by Mott, Zhang [35], Ang [36], Zheng [37], and others [38] for space charge-disordered semiconductors. Furthermore, a $p$ value of 1/2 was already reported by Efros [39], Overhof and Thomas [40], and more recently by Han et al. [41]. However, the reported values of the $p$ exponent values have not been clearly explained yet.

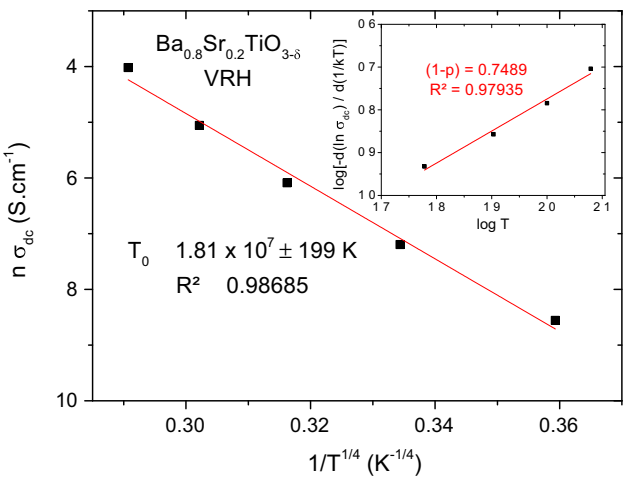


**Figure 8** Temperature dependence of dc bulk conductivity of $Ba_{0.8}Sr_{0.2}TiO_{3-\delta}$ nanoceramic.

The $p$ exponent can be deduced from the plot of $\log[-d(\ln\ \sigma_{dc})/d(1/kT)]$ versus $\log(T)$ expressed in Eq. 8 (see the inset of Fig. 8).

$$\log[-d(\ln \sigma_{dc})/d(1/kT)] = (1-p)\log T + A. \quad (8)$$

For $Ba_{0.8}Sr_{0.2}TiO_{3-\delta}$ the $p$ value determined here is 1/4. The value of $T_0$ is on the order of $1.81 \times 10^7$ K, which is lower than the value published by Zheng [37] for a $Ni_{0.5}Zn_{0.5}Fe_2O_4$ ceramic exhibiting colossal permittivity or by Ang [42] for Cu-doped $BaTiO_3$ following variable range hopping conduction mechanism. Considering the $\alpha$ value, which is on the order of magnitude of the lattice parameter ($\alpha = 0.4$ nm) and knowing the value of $T_0$ (from the fit of Fig. 8), it is then possible to calculate $N(E_F) = 7.6 \times 10^{19}$ $eV^{-1}$ $cm^{-3}$ from Eq. 7, which is in agreement with other authors [35–37], and the activation energies ($E_{A2}$) and the hopping distances ($R$) at different temperatures following the VRH model:

$$E_{A2} = 0.25kT_0^{1/4}T^{3/4} \quad (9)$$

$$R = [3\alpha/2\pi N(E_F)kT]^{1/4}. \quad (10)$$

The activation energies of the hopping process at low temperature are in the range of $0.022 \pm 0.002 \leq E_{A2} \leq 0.057 \pm 0.003$ eV, which is in the same order as low-temperature Debye's activation energy elsewhere reported [23]. In addition, the most probable hopping distance increases from 3.8 to 5.2 nm as the temperature decreases from 140 to 40 K. These distances that are approximately 10 times higher than the nearest neighbor distance, can be explained by the remarkably high concentration of polarons in the grains, allowing long-distance hopping to reach an equivalent site with comparable energy.

## Conclusions

The electrical properties of a series of $Ba_{1-x}Sr_xTiO_{3-\delta}$ nanoceramics ($0 \leq x \leq 1$) have been investigated. Colossal permittivity ($\sim 10^5$) with low losses ($\tan\delta = 0.03$) were achieved. All nanoceramics (except for $SrTiO_3$) follow the IBLC model used to represent grain and grain boundary responses. The grain conductivity decreases as Sr concentration increases. The hopping conductivity mechanisms were investigated in detail for two compounds: one Ba-rich ($Ba_{0.8}Sr_{0.2}TiO_{3-\delta}$) ceramic and one Sr-rich ($Ba_{0.2}Sr_{0.8}TiO_{3-\delta}$) ceramic. The Sr-rich ceramic exhibits a linear evolution of the *dc* grains conductivity versus $1/T$, which is in accordance with the NNH model, with an activation energy of $0.110 \pm 0.002$ eV. In Ba-rich compositions, the dc conductivity deviates from the $1/T$ law at low temperature, which is typical of a VRH mechanism. The use of VRH model, in better agreement with our results (compared to NNH model), indicates an increase of polaron activation energy (from $0.022 \pm 0.002$ to $0.057 \pm 0.003$ eV) and a decrease of hopping distances (from 5.2 to 3.8 nm) as the temperature increases from 40 to 140 K.

## Acknowledgements

This material is based upon work supported by the National Science Foundation under Grant No. DMR-1207293.

## Compliance with ethical standards

**Conflicts of interest** The authors declare that there is no conflict of interest in this manuscript.

## References

[1] O'Neill D, Bowman RM, Gregg JM (2000) Investigation into the dielectric behavior of ferroelectric superlattices formed by pulsed laser deposition. J Mater Sci: Mater Electron 11(7):537 541. doi:10.1023/a:1026539700710

[2] Zubko P, Stucki N, Lichtensteiger C, Triscone JM (2010) X ray diffraction studies of 180 degrees ferroelectric domains in $PbTiO_3/SrTiO_3$ superlattices under an applied electric field. Phys Rev Lett 104(18):4. doi:10.1103/PhysRevLett.104.187601

[3] Okatan MB, Misirlioglu IB, Alpay SP (2010) Contribution of space charges to the polarization of ferroelectric super lattices and its effect on dielectric properties. Phys Rev B 82(9):7. doi:10.1103/PhysRevB.82.094115

[4] Okatan MB, Mantese JV, Alpay SP (2010) Effect of space charge on the polarization hysteresis characteristics of monolithic and compositionally graded ferroelectrics. Acta Mater 58(1):39 48. doi:10.1016/j.actamat.2009.08.055

[5] Cole MW, Ngo E, Hubbard C, Hirsch SG, Ivill M, Sarney WL, Zhang J, Alpay SP (2013) Enhanced dielectric prop erties from barium strontium titanate films with strontium titanate buffer layers. J Appl Phys 114(16):10. doi:10.1063/1.4827421

[6] Tagantsev AK, Sherman VO, Astafiev KF, Venkatesh J, Setter N (2005) Erratum: ferroelectric materials for micro wave tunable applications (vol 11, pg 5). J Electroceram 14(3):199 203. doi:10.1007/s10832 005 0958 3

[7] Harigai T, Nam SM, Kakemoto H, Wada S, Saito K, Tsurumi T (2006) Structural and dielectric properties of perovskite type artificial superlattices. Thin Solid Films 509(1 2): 13 17. doi:10.1016/j.tsf.2005.09.008

[8] Subramanian MA, Li D, Duan N, Reisner BA, Sleight AW (2000) High dielectric constant in $ACu_3Ti_4O_{12}$ and $ACu_3$-$Ti_3FeO_{12}$ phases. J Solid State Chem 151(2):323 325. doi:10.1006/jssc.2000.8703

[9] Ramirez AP, Subramanian MA, Gardel M, Blumberg G, Li D, Vogt T, Shapiro SM (2000) Giant dielectric constant response in a copper titanate. Solid State Commun 115(5): 217 220. doi:10.1016/S0038 1098(00)00182 4

[10] Sinclair DC, Adams TB, Morrison FD, West AR (2002) $CaCu_3Ti_4O_{12}$: one step internal barrier layer capacitor. Appl Phys Lett 80(12):2153 2155. doi:10.1063/1.1463211

[11] Homes CC, Vogt T, Shapiro SM, Wakimoto S, Ramirez AP (2001) Optical response of high dielectric constant per ovskite related oxide. Science 293(5530):673 676

[12] Lunkenheimer P, Fichtl R, Ebbinghaus SG, Loidl A (2004) Nonintrinsic origin of the colossal dielectric constants in $CaCu_3Ti_4O_{12}$. Phys Rev B 70(17):4. doi:10.1103/PhysRevB.70.172102

[13] Wu JB, Nan CW, Lin YH, Deng Y (2002) Giant dielectric permittivity observed in Li and Ti doped NiO. Phys Rev Lett 89(21):4. doi:10.1103/PhysRevLett.89.217601

[14] Ikeda N, Ohsumi H, Ohwada K, Ishii K, Inami T, Kakurai K, Murakami Y, Yoshii K, Mori S, Horibe Y, Kito H (2005) Ferroelectricity from iron valence ordering in the charge frustrated system $LuFe_2O_4$. Nature 436(7054):1136 1138. doi:10.1038/nature04039

[15] Pronin AA, Torgashev VI, Bush AA, Gorshunov BP, Volkov AA, Prokhorov AS (2009) Low frequency dynamic response of the bismuth strontium ferrite (Bi, Sr)$FeO_3$ x. Phys Solid State 51(3):498 502. doi:10.1134/s106378340903010x

[16] Pecharroman C, Esteban Betegon F, Bartolome JF, Lopez Esteban S, Moya JS (2001) New percolative $BaTiO_3$ Ni composites with a high and frequency independent dielectric constant ($\varepsilon_r \approx 80{,}000$). Adv Mater 13(20):1541 1544. doi:10.1002/1521 4095(200110)13:20<1541:aid adma1541>3.0.co;2 x

[17] Guillemet Fritsch S, Boulos M, Durand B, Bley V, Lebey T (2005) Electrical characteristics of $BaTiO_3$ ceramics from hydrothermal prepared powders. J Eur Ceram Soc 25(12):2749 2753. doi:10.1016/j.jeurceramsoc.2005.03.133

[18] Lunkenheimer P, Bobnar V, Pronin AV, Ritus AI, Volkov AA, Loidl A (2002) Origin of apparent colossal dielectric constants. Phys Rev B 66(5):4. doi:10.1103/PhysRevB.66.052105

[19] Li W, Schwartz RW (2007) Maxwell Wagner relaxations and their contributions to the high permittivity of calcium copper titanate ceramics. Phys Rev B 75(1):4. doi:10.1103/PhysRevB.75.012104

[20] Fang TT, Liu CP (2005) Evidence of the internal domains for inducing the anomalously high dielectric constant of $CaCu_3Ti_4O_{12}$. Chem Mater 17(20):5167 5171. doi:10.1021/cm051180k

[21] Han H, Voisin C, Guillemet Fritsch S, Dufour P, Tenailleau C, Turner C, Nino JC (2013) Origin of colossal permittivity in $BaTiO_3$ via broadband dielectric spectroscopy. J Appl Phys 113(2):8. doi:10.1063/1.4774099

[22] Koops CG (1951) On the dispersion of resistivity and dielectric constant of some semiconductors at audio frequencies. Phys Rev 83(1):121 124. doi:10.1103/PhysRev.83.121

[23] Dupuis S, Sulekar S, Kim JH, Han H, Dufour P, Tenailleau C, Nino JC, Guillemet Fritsch S (2016) Colossal permittivity and low losses in $Ba_{1-x}Sr_xTiO_{3-\delta}$ reduced nanoceramics. J Eur Ceram Soc 36(3):567 575. doi:10.1016/j.jeurceramsoc.2015.10.017

[24] Valdez Nava Z, Guillemet Fritsch S, Tenailleau C, Lebey T, Durand B, Chane Ching JY (2009) Colossal dielectric permittivity of $BaTiO_3$ based nanocrystalline ceramics sintered by spark plasma sintering. J Electroceram 22(1 3):238 244. doi:10.1007/s10832 007 9396 8

[25] Voisin C, Guillemet Fritsch S, Dufour P, Tenailleau C, Han H, Nino JC (2013) Influence of oxygen substoichiometry on the dielectric properties of $BaTiO_{3-\delta}$ nanoceramics obtained by spark plasma sintering. Int J Appl Ceram Technol 10:E122 E133. doi:10.1111/ijac.12058

[26] Guillemet Fritsch S, Valdez Nava Z, Tenailleau C, Lebey T, Durand B, Chane Ching JY (2008) Colossal permittivity in ultrafine grain size $BaTiO_{3-x}$ and $Ba_{0.95}La_{0.05}TiO_{3-x}$ materials. Adv Mater 20(3):551 555. doi:10.1002/adma.200700245

[27] Schneider CA, Rasband WS, Eliceiri KW (2012) NIH image to ImageJ: 25 years of image analysis. Nat Methods 9(7): 671 675. doi:10.1038/nmeth.2089

[28] Zheng H, Li L, Xu ZJ, Weng WJ, Han GR, Ma N, Du PY (2013) Ferroelectric/ferromagnetic ceramic composite and its hybrid permittivity stemming from hopping charge and conductivity inhomogeneity. J Appl Phys 113(4):8. doi:10.1063/1.4781100

[29] Jonscher AK (1975) Physical basis of dielectric loss. Nature 253(5494):717 719. doi:10.1038/253717a0

[30] Jonscher AK (1992) The universal dielectric response and its physical significance. IEEE Trans Electr Insul 27(3):407 423. doi:10.1109/14.142701

[31] Goryunova NA, Kolomiets BT (1956) New vitreous semi conductors. Izv Akad nauk SSSR, ser fiz 20(12):1496 1500
[32] Miller A, Abrahams E (1960) Impurity conduction at low concentrations. Phys Rev 120(3):745 755. doi:10.1103/PhysRev.120.745
[33] Jonker GH (1959) Analysis of the semiconducting properties of cobalt. J Phys Chem Solids 9(2):165 175. doi:10.1016/0022 3697(59)90206 9
[34] Mott NF, Davis EA (1979) Electronic processes in non crystalline materials, 2nd edn. Clarendon Press, Oxford
[35] Zhang L, Tang ZJ (2004) Polaron relaxation and variable range hopping conductivity in the giant dielectric constant material $CaCu_3Ti_4O_{12}$. Phys Rev B 70(17):6. doi:10.1103/PhysRevB.70.174306
[36] Ang C, Yu Z, Jing Z (2000) Dielectric spectra and electrical conduction in Fe doped $SrTiO_3$. Phys Rev B 61(6):3922 3926. doi:10.1103/PhysRevB.61.3922
[37] Zheng H, Weng WJ, Han GR, Du PY (2013) Colossal permittivity and variable range hopping conduction of polarons in $Ni_{0.5}Zn_{0.5}Fe_2O_4$ ceramic. J Phys Chem C 117(25):12966 12972. doi:10.1021/jp402320b
[38] Kastner MA, Birgeneau RJ, Chen CY, Chiang YM, Gabbe DR, Jenssen HP, Junk T, Peters CJ, Picone PJ, Thio T, Thurston TR, Tuller HL (1988) Resistivity of nonmetallic $La_{2-y}Sr_yCu_{1-x}LiO_{4-\delta}$ single crystals. Phys Rev B 37(1):111 117. doi:10.1103/PhysRevB.37.111
[39] Efros AL, Shklovskii BI (1975) Coulomb gap and low temperature conductivity of disordered systems. J Phys C Solid State Phys 8(4):L49 L51. doi:10.1088/0022 3719/8/4/003
[40] Overhof H, Thomas P (1989) Electronic transport in hydrogenated amorphous semiconductors introduction. Springer Tracts Mod Phys 114:1 167
[41] Han HS, Davis C, Nino JC (2014) Variable range hopping conduction in $BaTiO_3$ ceramics exhibiting colossal permittivity. J Phys Chem C 118(17):9137 9142. doi:10.1021/jp502314r
[42] Ang C, Jing Z, Yu Z (1999) Variable range hopping conduction and metal insulator transition in Cu doped $BaTiO_3$. J Phys: Condens Matter 11(48):9703 9708. doi:10.1088/0953 8984/11/48/327